Electronic Supplementary Material (ESI) for Journal of Materials Chemistry C.

Supporting Information

For

Multichannel charge transfer enhanced radiative decay and RISC in TADF material containing multiple donors and acceptors

Zhaolong He,[a] Jiuyan Li,[a]* Di Liu,[a,b]* Huihui Wan,[c] Yongqiang Mei,[a] Chunlong Shi[a]

[a] Frontiers Science Center for Smart Materials, College of Chemical Engineering, Dalian University of Technology, 2 Linggong Road, Dalian, 116024, China. E-mail: jiuyanli@dlut.edu.cn, liudi@dlut.edu.cn

[b] State Key Laboratory of Luminescent Materials and Devices, South China University of Technology, Guangzhou, 510640, China.

[c] Instrumental Analysis Center, Dalian University of Technology, Dalian, 116024, China.

Contents

1. Instruments and methods

1.1 General Information. Bruker Avance II 400 was used to record ^{1}H and NMR data based on tetramethylsilane (TMS) as internal standard and chloroform-d ($CDCl_3$) as the solvent. The high-resolution mass (HRMS) spectra were measured using LTQ Orbitrap XL for HRMS-ESI. The electrochemical workstation (BAS100B, USA) and the traditional three-electrode configuration, including a glass-carbon electrode, a Pt-wire, and a saturated calomel electrode (SCE) were used to measure the electrochemical performance of cyclic voltammetry (CV) at a scan rate of 100 mV s^{-1}. The samples in dichloromethane (DCM, anodic) or *N*, *N*-dimethylformamide (DMF, cathodic) solutions containing 0.1 M $[Bu_4N]PF_6$ as the electrolyte were deoxygenated with nitrogen for 10 mins before scanning. The UV-vis absorption spectra were measured on Perkin-Elmer Lambda 650 spectrophotometer. The fluorescence spectra at room temperature and the temperature-dependent transient PL spectra were obtained from the Edinburgh FLS1000 fluorescence spectrophotometer while the phosphorescence spectra were recorded using a Hitachi F-7000 fluorescence spectrometer at 77 K in 2-MeTHF. Photoluminescence quantum yields (PLQYs) were measured on a HAMAMATSU absolute PL quantum yield spectrometer C11347.

The density functional theory (DFT) calculation at the B3LYP-D3BJ/def2-SVP level was used to optimize the ground state geometries of the investigated molecules. Time-dependent density functional theory (TD-DFT) calculations were performed at PBE0/def2-SVP using the optimized ground state geometries. The hole/particle were

deduced from the natural transition orbitals (NTOs) analysis based on TD-DFT results.[1] The spin-orbit coupling matrix elements (SOCME) were calculated by ORCA program. Independent gradient model based on Hirshfeld partition of molecular density (IGMH) method is a visual analysis of chemical systems interactions, wherein $\delta g = \delta g^{inter} + \delta g^{intra}$, δg represents interactions between all atoms in the current system, δg^{inter} and δg^{intra} represent interactions of interfragment and intrafragment, respectively. Sign $(\lambda_2)\rho$ were calculated and visualized using Multiwfn and VMD.[2, 3]

1.2 OLED fabrication and measurements. The pre-cleaned ITO glass substrates with the sheet resistance of 15 Ω m^{-2} were treated by UV-ozone for 30 minutes. A 40 nm thick PEDOT: PSS film was first spin-coated on the ITO glass substrate and baked in the air at 120 ℃ for 30 minutes. The substrate was then transferred to a vacuum chamber where the organic layers were deposited at a basic pressure of less than 10^{-6} Torr (1 Torr =133.32 Pa). Finally, a 1 nm thin layer of LiF film was deposited on the organic layers, and then 200 nm Al film was deposited as the cathode. The overlap part of the two electrodes was the emission area of each pixel, which was 9 mm^2. A PR705 photometer and source-measure-unit Keithley 236 were used to measure the EL spectra, CIE coordinates, and *J-V-B* curves of the devices under ambient conditions. The forward-viewing external quantum efficiency was calculated with an assumption of a Lambertian emission profile by using the current efficiency, EL spectra, and human photopic sensitivity.

1.3 Calculation of the rate constants of the different kinetic processes

The following formula were used for calculations:

$$\Phi = \Phi_{PF} + \Phi_{DF} \quad \text{(E1)}$$

$$k_r = \Phi_{PF}/\tau_{PF} \quad \text{(E2)}$$

$$\Phi = k_r/(k_r + k_{nr}) \quad \text{(E3)}$$

$$\Phi_{PF} = k_r/(k_r + k_{isc} + k_{nr}) \quad \text{(E4)}$$

$$k_{risc} = k_p k_d \Phi_{DF}/k_{isc}\Phi_{PF} \quad \text{(E5)}$$

$$k_p = \frac{1}{\tau_{PF}} \quad \text{(E6)}$$

$$k_d = \frac{1}{\tau_{DF}} \quad \text{(E7)}$$

k_r, k_{nr}, k_{isc}, and k_{risc} represent the rate constants of radiative, non-radiative, intersystem crossing (ISC) and RISC, respectively. Φ, Φ_{PF}, and Φ_{DF} represent total PLQY, PLQY of the prompt component and delayed component, respectively. τ_{PF} and τ_{DF} are lifetimes of the prompt and delayed components, respectively.[4] Φ, τ_{PF}, and τ_{DF} were measured experimentally.[4, 5] All data are shown in Table 1.

2. Compound synthesis

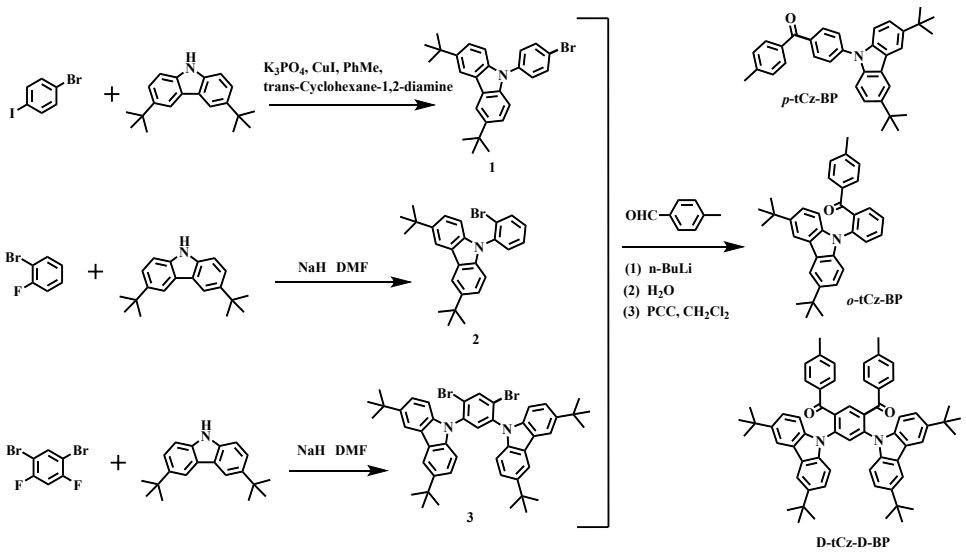

Scheme S1 Structures and synthetic routes of *p*-tCz-BP, *o*-tCz-BP and D-tCz-D-BP.

The key intermediates of 1, 2 and 3 were synthesized according to the literature methods.[6-8]

General procedure for synthesis of (4-(3,6-di-tert-butyl-9H-carbazol-9-yl)phenyl)(p-tolyl)methanone (p-tCz-BP*), (2-(3,6-di-tert-butyl-9H-carbazol-9-yl)phenyl)(p-tolyl)methanone (o*-tCz-BP*) and (4,6-bis(3,6-di-tert-butyl-9H-carbazol-9-yl)-1,3-phenylene)bis(p-tolylmethanone) (*D-tCz-D-BP*).* Compound 1 (2.3 g, 5.3 mmol) was added to dry THF in a three-necked flask under nitrogen. The solution was cooled to -78 ℃, and 2.5 mL of n-BuLi (2.5 M) was added dropwise using a syringe. The mixture was stirred for 1 h at -78 ℃ and then 4-methylbenzaldehyde (10.6 mmol) was slowly added into the reaction solution. The mixture was stirred for 1 h at -78 ℃ and then stirred overnight at room temperature. Subsequently, the mixture was stirred for 10 minutes under ice-water. Then, 50 mL of ice water was added to quench the reaction and perform a hydrolysis reaction. The resulting mixture was extracted with dichloromethane three times. The combined organic layers were

dried over anhydrous magnesium sulfate. After filtration and solvent evaporation, the crude product that without further purification or characterization was dissolved in 40 mL of dichloromethane in a 100 mL round bottom flask, then pyridinium chlorochromate (PCC) (4.7 g, 21.8 mmol) was added. The mixture was stirred for 12 h. The precipitate was filtered and the filtrate was poured into saturated saltwater and extracted with dichloromethane. The organic layer was then collected, dried with magnesium sulfate, filtered, and evaporated under reduced pressure. After solvent evaporation, the crude product was purified by column chromatography over silica gel with a dichloromethane/petroleum ether (1 : 30 v/v) mixture as an eluent.

p-tCz-BP: white solid, yield 40%. ^{1}H NMR (400 MHz, $CDCl_3$) δ 8.15 (s, 2H), 8.03 (d, J = 8.2 Hz, 2H), 7.82 (d, J = 7.8 Hz, 2H), 7.71 (d, J = 8.2 Hz, 2H), 7.51 – 7.46 (m, 4H), 7.35 (d, J = 7.8 Hz, 2H), 2.48 (s, 3H), 1.48 (s, 18H). HRMS-ESI (*m/z*): cal. for $C_{34}H_{35}NO$ 473.2719; Found: 474.2785 $[M+H]^+$. Anal. calcd for $C_{34}H_{35}NO$: C, 86.22; H, 7.45; N, 2.96; Found: C, 86.24; H, 7.49; N, 2.98.

o-tCz-BP: white solid, yield 35%. ^{1}H NMR (400 MHz, $CDCl_3$) δ 7.83 (d, J = 7.9 Hz, 1H), 7.79 (d, J = 1.4 Hz, 2H), 7.77 – 7.73 (m, 1H), 7.62 – 7.58 (m, 2H), 7.39 (s, 1H), 7.36 (d, J = 2.5 Hz, 1H), 7.14 (s, 1H), 7.12 (s, 1H), 6.86 (d, J = 8.1 Hz, 2H), 6.46 (d, J = 7.9 Hz, 2H), 2.03 (s, 3H), 1.42 (s, 18H). HRMS-ESI (*m/z*): cal. for $C_{34}H_{35}NO$ 473.2719; Found: 474.2790 $[M+H]^+$. Anal. calcd for $C_{34}H_{35}NO$: C, 86.22; H, 7.45; N, 2.96; Found: C, 86.24; H, 7.51; N, 2.98.

D-tCz-D-BP: pale-yellow solid, yield 30%. ^{1}H NMR (400 MHz, $CDCl_3$) δ 8.32 (s, 1H), 7.91 (s, 1H), 7.81 (s, 4H), 7.44 (d, J = 8.6 Hz, 4H), 7.31 (d, J = 8.6 Hz, 4H),

7.02 (d, J = 8.0 Hz, 4H), 6.54 (d, J = 7.9 Hz, 4H), 2.08 (s, 6H), 1.43 (s, 36H). HRMS-ESI (m/z): cal. for $C_{62}H_{64}N_2O_2$ 868.4968; Found: 891.4855 $[M+Na]^+$. Anal. calcd for $C_{62}H_{64}N_2O_2$: C, 85.67; H, 7.42; N, 3.22; Found: C, 85.69; H, 7.50; N, 3.20.

3. Supplementary Figures and Tables

Table S1 The corresponding energy levels of *p*-tCz-BP, *o*-tCz-BP and D-tCz-D-BP.

Compound	LUMO+1 [eV]	LUMO [eV]	HOMO [eV]	HOMO-1 [eV]	HOMO-2 [eV]	HOMO-3 [eV]
p-tCz-BP	-0.98	-1.98	-5.54	-5.90	-6.81	-6.88
o-tCz-BP	-0.87	-1.93	-5.32	-5.63	-6.62	-6.88
D-tCz-D-BP	-1.89	-2.25	-5.41	-5.48	-5.74	-5.74

Table S2 Spin-orbit coupling matrix elements (SOCME) of *p*-tCz-BP, *o*-tCz-BP and D-tCz-D-BP.

Compound	SOC (cm^{-1})	T_1	T_2	T_3	T_4	T_5	T_6
p-tCz-BP	S_1	0.694	0.546	1.040	0.349	0.820	0.132
	S_2	0.280	0.276	0.553	0.395	0.241	0.045
	S_3	16.741	12.938	21.283	0.132	10.631	0.268
	S_4	0.214	0.251	0.226	0.082	0.094	0.195
	S_5	0.638	0.779	0.122	0.105	0.066	0.030
	S_6	0.494	0.352	0.610	0.199	0.221	0.022
	S_1	0.357	8.033	1.030	6.168	0.033	1.814
	S_2	1.093	1.083	1.074	2.776	0.099	0.769

	S_3	3.644	23.957	4.796	24.638	0.111	5.872
	S_4	1.669	2.602	0.561	0.668	0.031	0.248
	S_5	0.457	2.684	0.572	0.491	0.103	0.177
	S_6	2.430	0.441	0.277	0.345	0.037	1.845
D-tCz-D-BP	S_1	0.133	1.305	2.637	0.932	2.678	2.458
	S_2	1.269	0.151	0.520	0.660	0.738	2.051
	S_3	0.425	0.257	0.574	0.333	0.592	1.341
	S_4	0.082	0.293	0.435	0.321	0.574	0.935
	S_5	1.012	0.369	2.534	0.896	2.436	1.840
	S_6	0.334	0.571	3.490	1.980	3.709	5.164

Table S3 Crystal data and structure refinement for D-tCz-D-BP.

Identification code	D-tCz-D-BP
Empirical formula	$C_{62}H_{64}N_2O_2$
CCDC No.	2174202
Formula weight	869.15
Temperature/K	200
Space group	P1
a (Å)	11.744(6)
b (Å)	12.517(9)
c (Å)	18.534(10)
α (°)	91.23(2)
β (°)	106.013(8)
γ (°)	101.022(9)
Volume(Å3)	2563(3)
Z	2
F(000)	932.0
Data completeness	0.985

Table S4 Experimentally determined physical parameters of *p*-tCz-BP, *o*-tCz-BP and D-tCz-D-BP.

Compound	λ_{abs}[a] [nm]	λ_{em}[a] [nm]	E_S/E_T[b] [eV]	ΔE_{ST}[c] [eV]	HOMO /LUMO[d] [eV]	E_g[d] [eV]
p-tCz-BP	296, 330, 347, 363	467	3.10/2.87	0.23	-5.55/-2.79	2.76
o-tCz-BP	296, 330, 341, 370	485	3.00/2.92	0.08	-5.52/-2.67	2.85
D-tCz-D-BP	296, 330, 344, 381	450,530	2.86/2.71	0.15	-5.58/-2.89	2.69

[a] Absorption and PL peak wavelengths in dilute toluene solution at RT. [b] Measured from the highest-energy onset wavelengths of steady state PL spectra (RT) and phosphorescence spectra (with ideally 60ms delay time following pulsed excitation) in 8 wt% doped PPF films. [c] Energy splitting between S_1 and T_1 estimated as $\Delta E_{ST} = E_S - E_T$. [d] HOMO and LUMO energy levels determined from the electrochemical oxidation and reduction potentials.

Table S5 Summary of the key performances of the reported TBCT and TSCT type TADF-OLEDs in recent years.

Emitter	EL (nm)	EQE (%)	Ref.
***o*-tCz-BP**	**468**	**11.1**	**This work**
D-tCz-D-BP	**490**	**24.9**	**This work**
SF12oTz	496	22.4	9
SF23oTz	484	19.6	9
SF34oTz	482	14.6	9
1CTF	490	17.5	10
2CTF	503	19.8	10
3CTF	508	22.6	10
*o*B-2Cz	486	28.1	11
*o*B-2*t*Cz	498	27.5	11
TP-BP-DMAC	488	20.5	12
TP-BP-PXZ	531	13.8	12
SFO-SPAC	502	23.5	13
SFO-DMAC	532	15.6	13
T-CNDF-T-tCz	484	21.0	14
S-CNDF-S-tCz	466	2.6	14
S-CNDF-D-tCz	466	3.7	14
4Cz-DPS	524	20.7	15
2Cz-DPS	518	28.7	15

Table S6 Summary of the key performances of TADF molecule act as emitter, host

and host emitter in OLEDs.

Compound	EQE/CIE[a]	EQE/CIE[b]	EQE/CIE[c]	Ref.
D-tCz-D-BP	**24.9%**	**21.0%**	**18.8%**	**This**
	(0.22,0.40)	**(0.62,0.36)**	**(0.41,0.42)**	**work**
DCB-BP-SFAC	23.5%	13.6%	17.8%	[16]
	(0.199,0.417)	(0.658,0.326)	(0.333,0.397)	
SBF-BP-DMAC	24.5%	26.8%	21.0%	[17]
	(0.308,0.570)	(0.477,0.518)	(0.442,0.493)	
Tri-o-2PO	--	22.1%	21.1%	[18]
	--	--	(0.38,0.45)	
o-CzTrz	17.5%	13.9%	20.3%	[19]
	(0.21,0.43)	(0.28,0.56)	(0.34,0.42)	
m-CzTrz	19.2%	20.8%	19.8%	[19]
	(0.25,0.44)	(0.31,0.62)	(0.38,0.50)	

[a] Compound served as emitter for doped OLED. [b] Compound served as host for PhOLED. [c] Compound served as host emitter for single emissive layer WOLED.

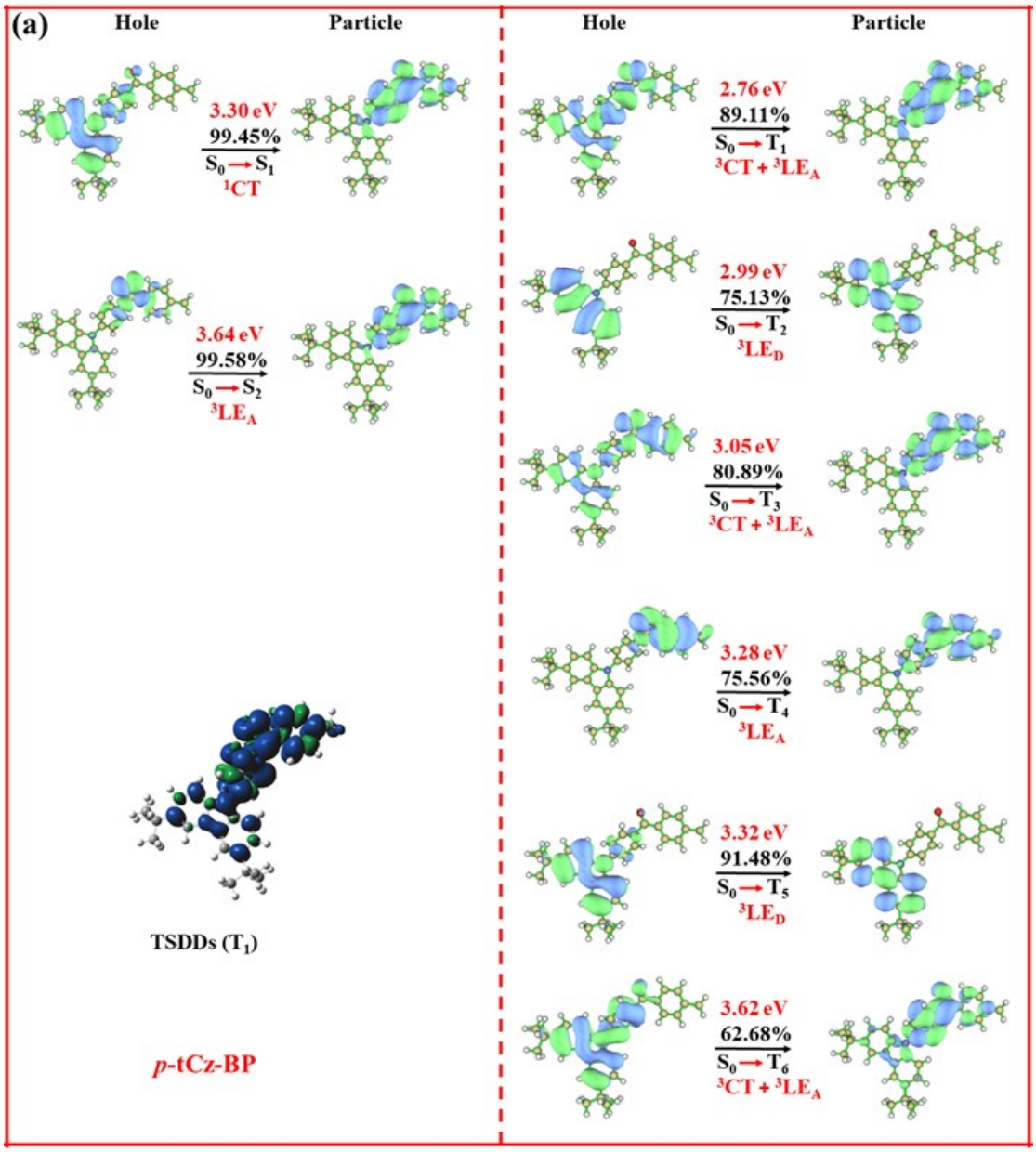
(a)
Hole
Particle
3.30 eV
99.45%
S0 → S1
1CT
3.64 eV
99.58%
S0 → S2
3LEA
TSDDs (T1)
p-tCz-BP
Hole
Particle
2.76 eV
89.11%
S0 → T1
3CT + 3LEA
2.99 eV
75.13%
S0 → T2
3LED
3.05 eV
80.89%
S0 → T3
3CT + 3LEA
3.28 eV
75.56%
S0 → T4
3LEA
3.32 eV
91.48%
S0 → T5
3LED
3.62 eV
62.68%
S0 → T6
3CT + 3LEA

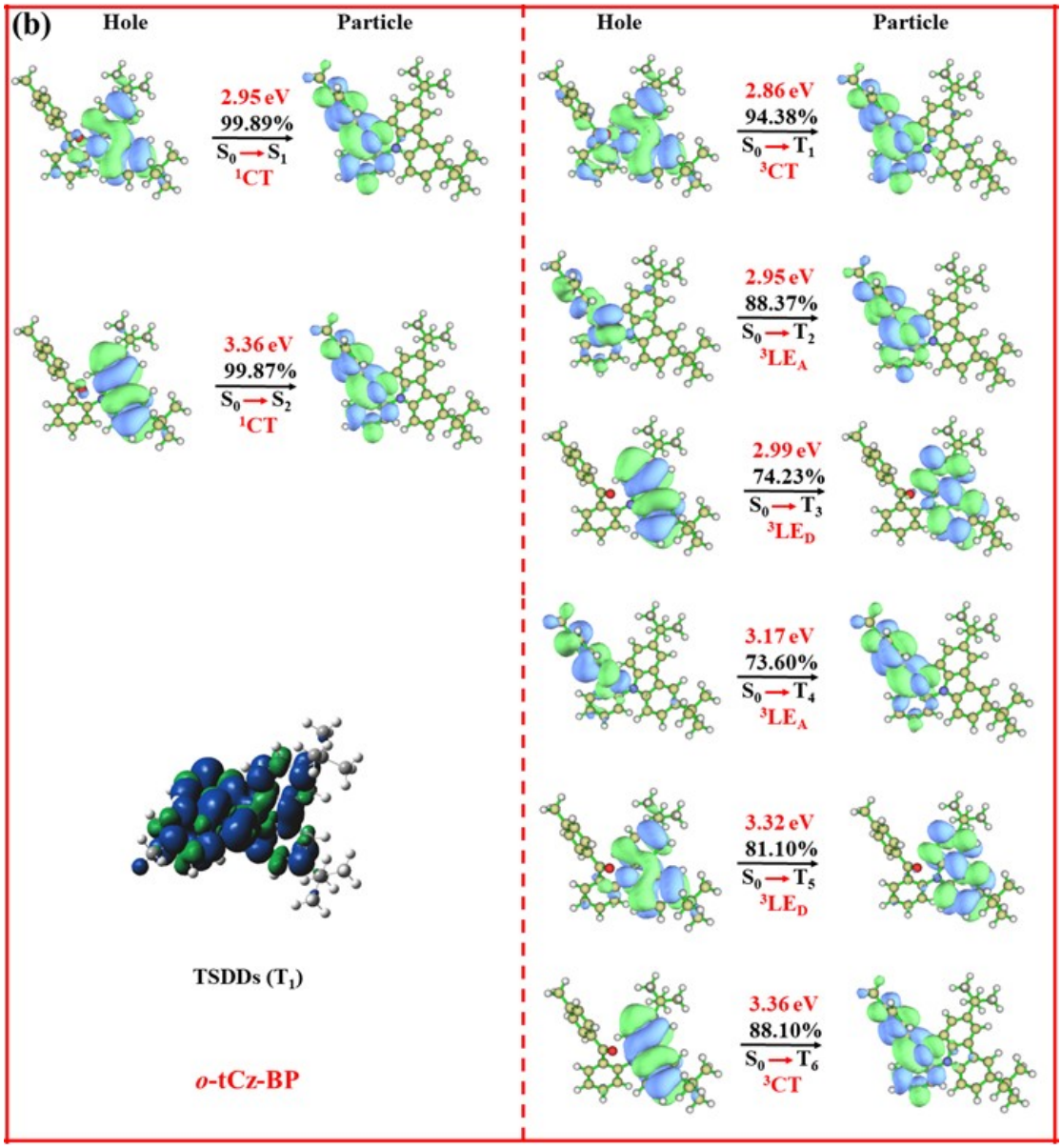
(b)
Hole
Particle
2.95 eV
99.89%
S0 → S1
1CT
3.36 eV
99.87%
S0 → S2
1CT
TSDDs (T1)
o-tCz-BP
Hole
Particle
2.86 eV
94.38%
S0 → T1
3CT
2.95 eV
88.37%
S0 → T2
3LEA
2.99 eV
74.23%
S0 → T3
3LED
3.17 eV
73.60%
S0 → T4
3LEA
3.32 eV
81.10%
S0 → T5
3LED
3.36 eV
88.10%
S0 → T6
3CT

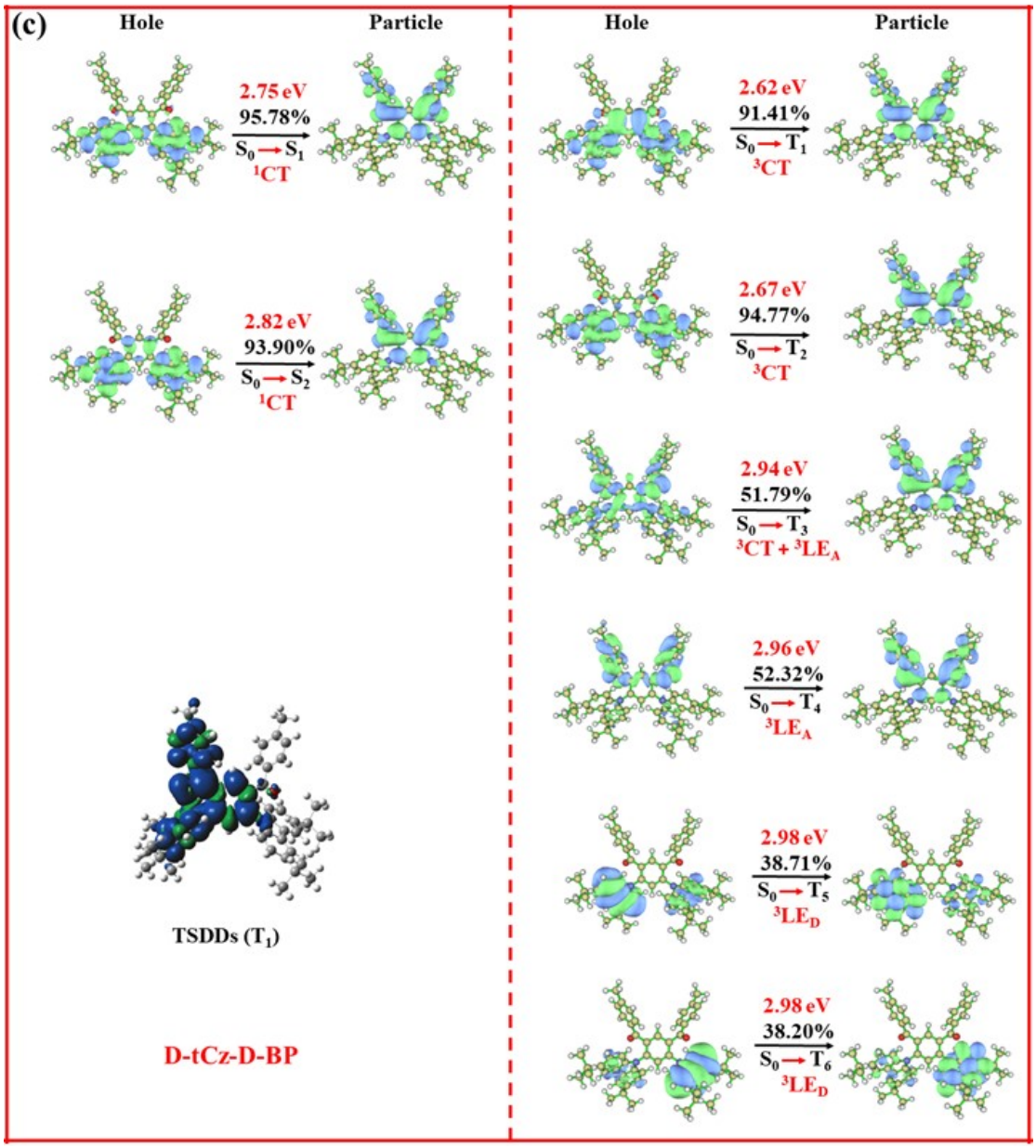

Fig. S1 The NTO calculations and TSDDs (T_1) of *p*-tCz-BP, *o*-tCz-BP and D-tCz-D-BP.

(a)

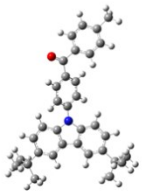

p-tCz-BP

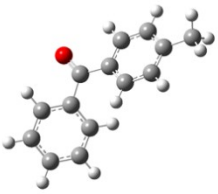

Fragment A

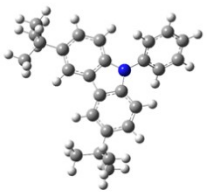

Fragment D

Excited state	*p*-tCz-BP					
S	3.30	3.64	3.71	4.05	4.29	4.52
T	2.76	2.99	3.05	3.28	3.32	3.62

Excited state	Fragment A					
S	3.64	4.72	4.73	4.80	5.07	5.48
T	2.90	3.27	3.32	4.10	4.15	4.25

Excited state	Fragment D					
S	4.02	4.24	4.40	4.53	4.68	4.95
T	3.00	3.27	3.32	3.89	3.94	4.08

(b)

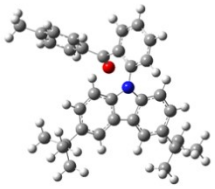

o-tCz-BP

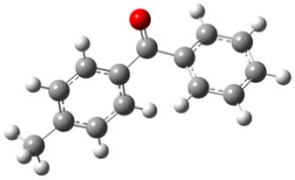

Fragment A

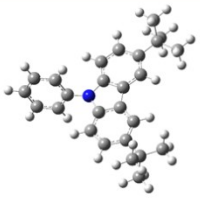

Fragment D

Excited state	*o*-tCz-BP					
S	2.95	3.36	3.66	3.97	4.05	4.12
T	2.86	2.95	2.99	3.17	3.32	3.36

Excited state	Fragment A					
S	3.69	4.79	4.85	4.89	5.05	5.50
T	2.99	3.20	3.45	4.10	4.26	4.35

Excited state	Fragment D					
S	4.05	4.14	4.31	4.53	4.63	4.79
T	3.00	3.29	3.42	3.90	3.94	4.13

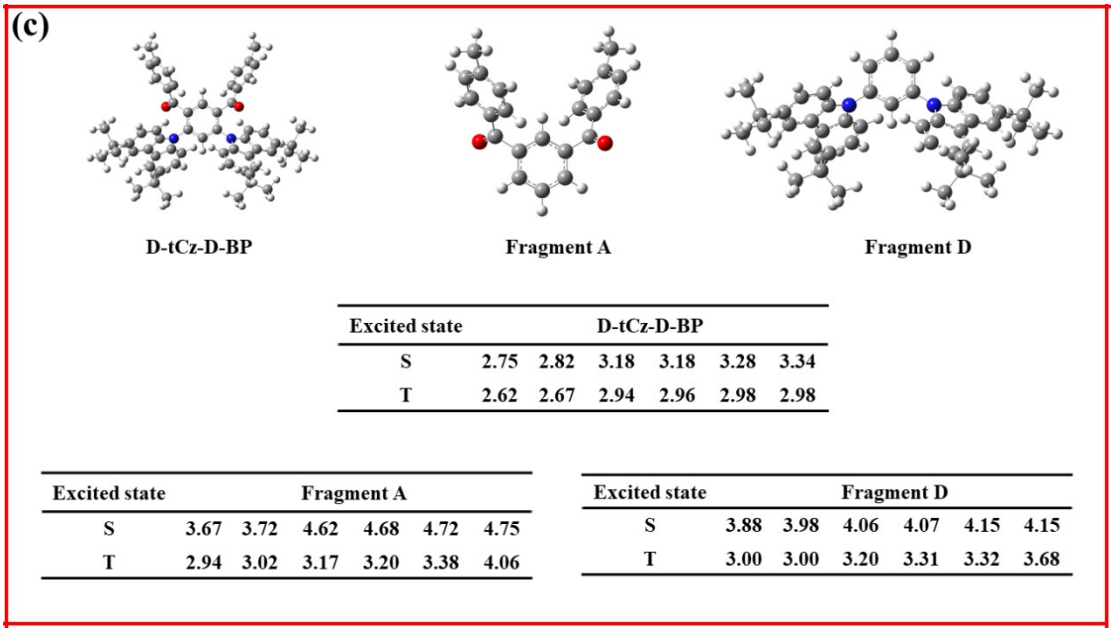

Excited state	D-tCz-D-BP					
S	2.75	2.82	3.18	3.18	3.28	3.34
T	2.62	2.67	2.94	2.96	2.98	2.98

Excited state	Fragment A					
S	3.67	3.72	4.62	4.68	4.72	4.75
T	2.94	3.02	3.17	3.20	3.38	4.06

Excited state	Fragment D					
S	3.88	3.98	4.06	4.07	4.15	4.15
T	3.00	3.00	3.20	3.31	3.32	3.68

Fig. S2 The excited state energy-levels of corresponding fragment molecules based on the optimized ground geometries of *p*-tCz-BP, *o*-tCz-BP and D-tCz-D-BP.

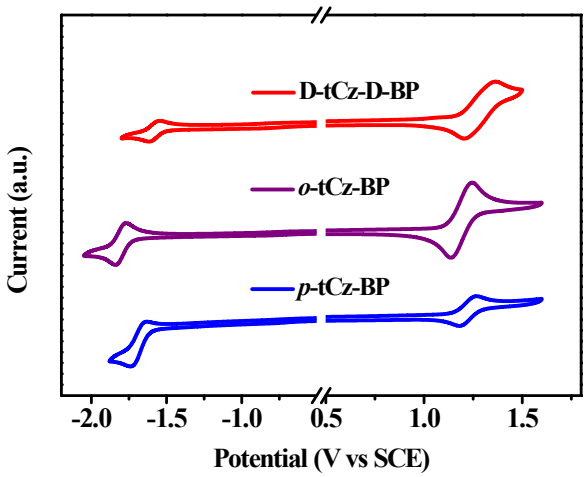

Fig. S3 Cyclic voltammograms of *p*-tCz-BP, *o*-tCz-BP and D-tCz-D-BP.

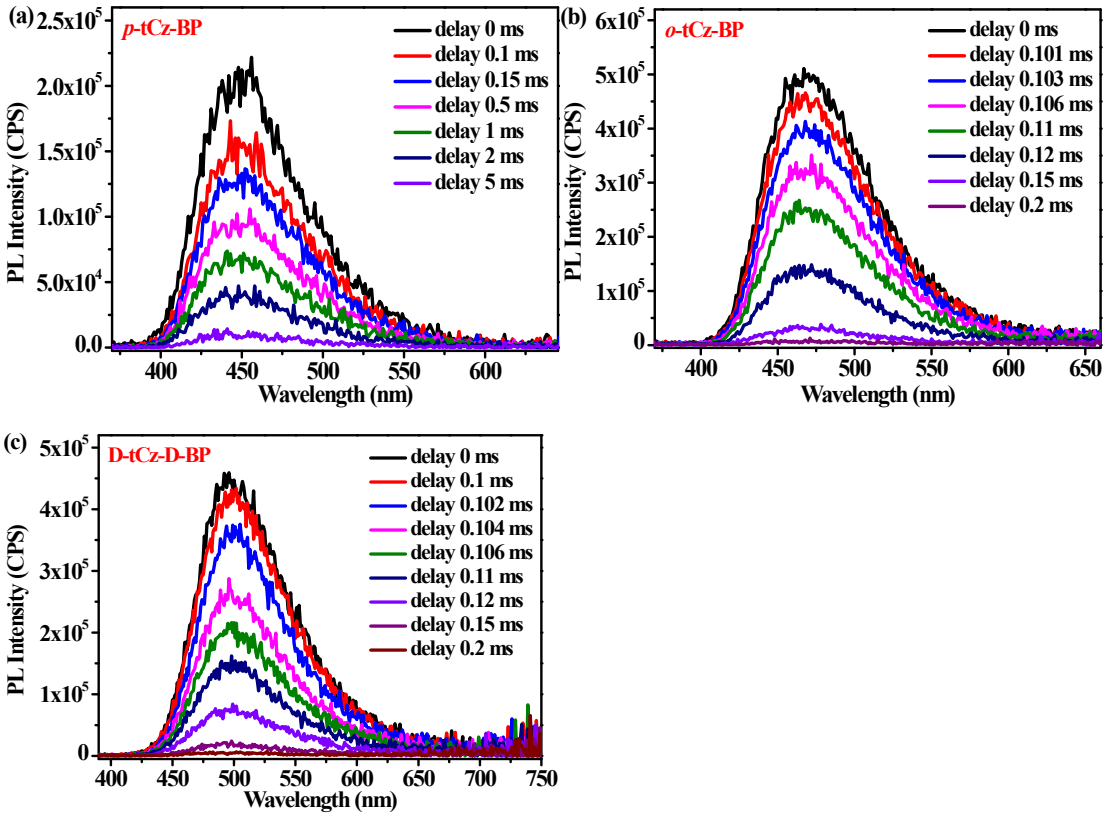

Fig. S4 Time-resolved PL spectra of (a) *p*-tCz-BP, (b) *o*-tCz-BP, and (c) D-tCz-D-BP in 8 wt% doped PPF films at different delay time.

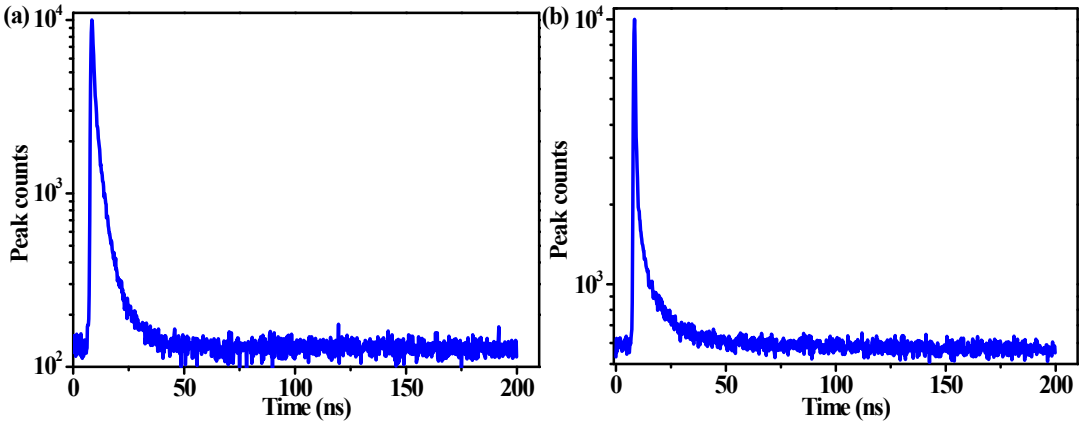

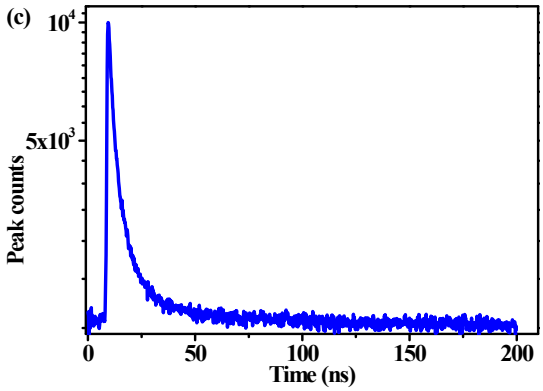

Fig. S5 Decay curve of prompt fluorescence at room temperature for (a) *p*-tCz-BP, (b) *o*-tCz-BP and (c) D-tCz-D-BP in 8 wt% doped PPF films.

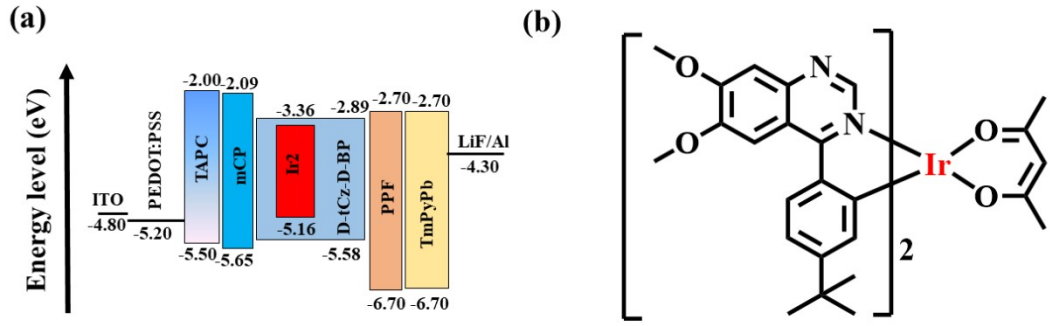

Fig. S6 (a) Device configuration and energy level diagrams of WOLED, (b) Chemical structures of Ir2.

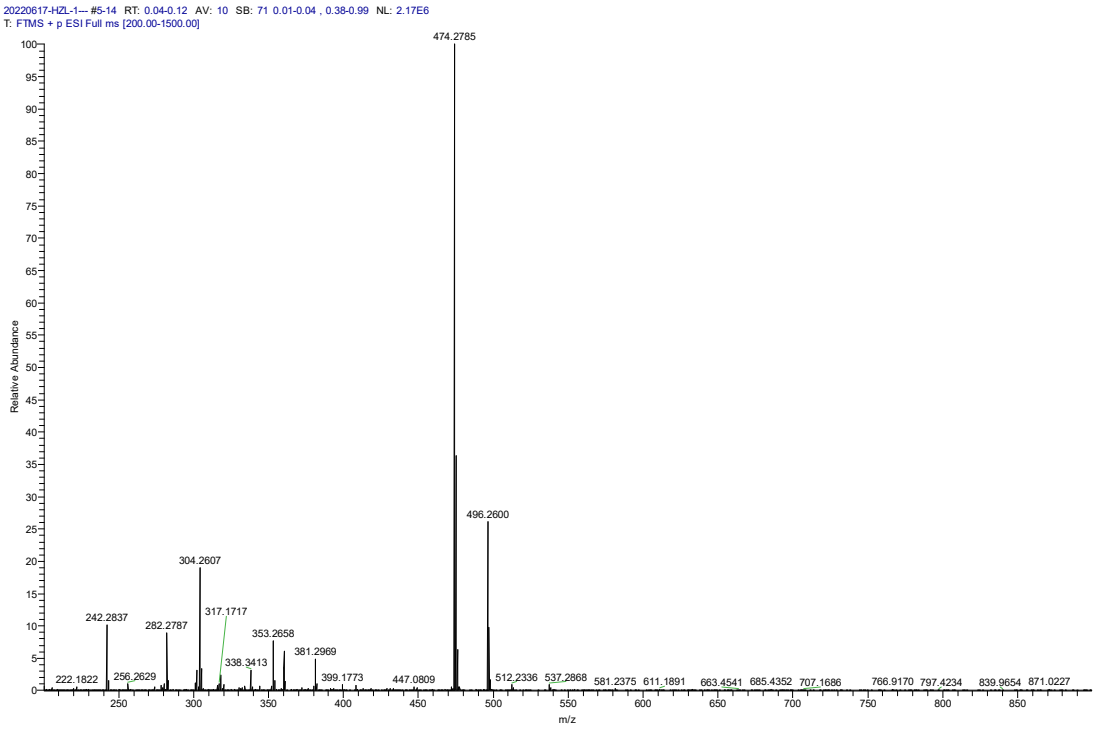

Fig. S7 MS spectrum of *p*-tCz-BP.

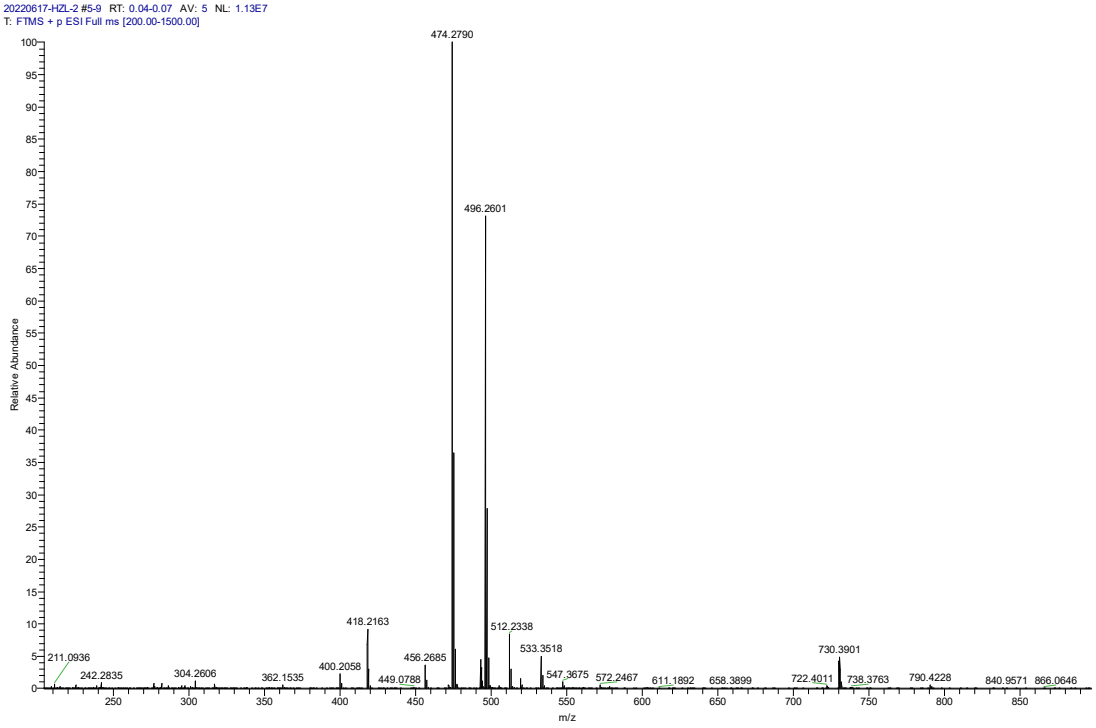

Fig. S8 MS spectrum of *o*-tCz-BP.

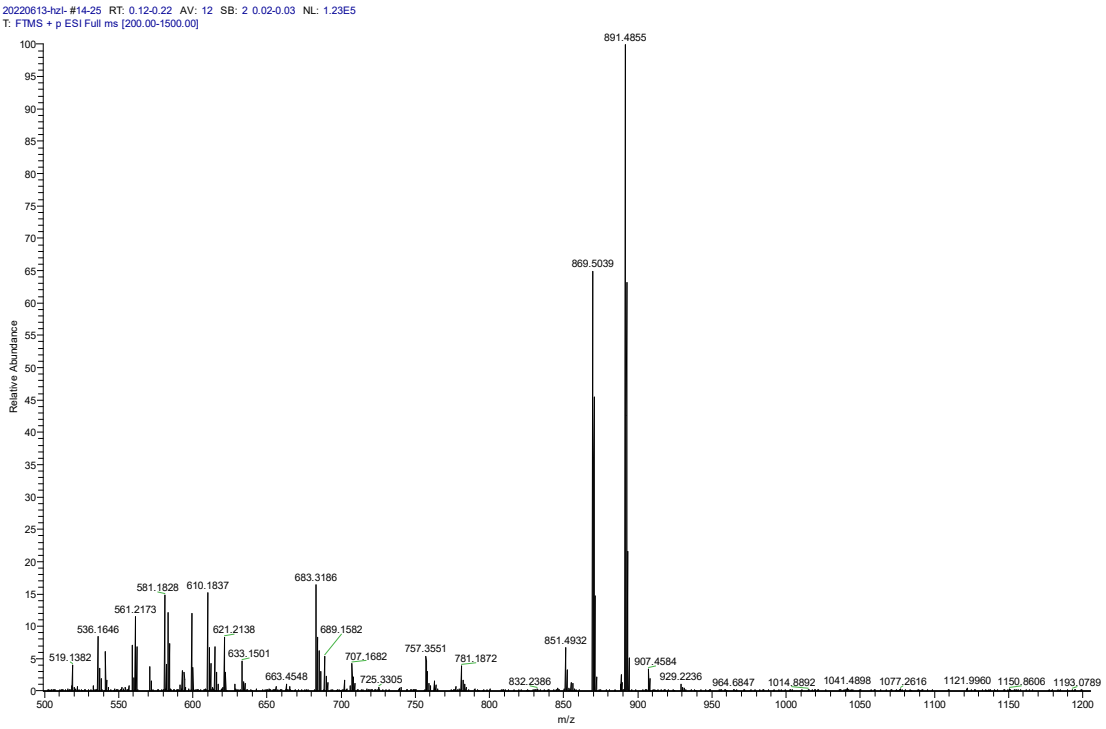

Fig. S9 MS spectrum of D-tCz-D-BP.

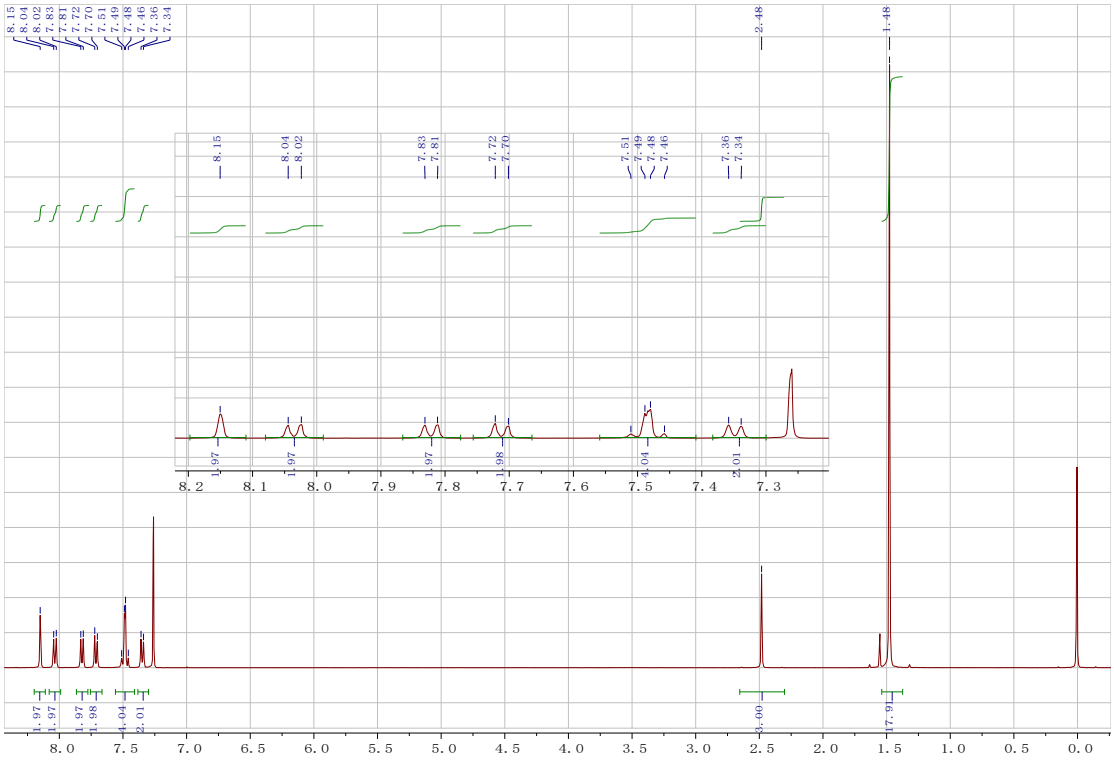

Fig. S10 ^{1}H NMR spectrum of *p*-tCz-BP.

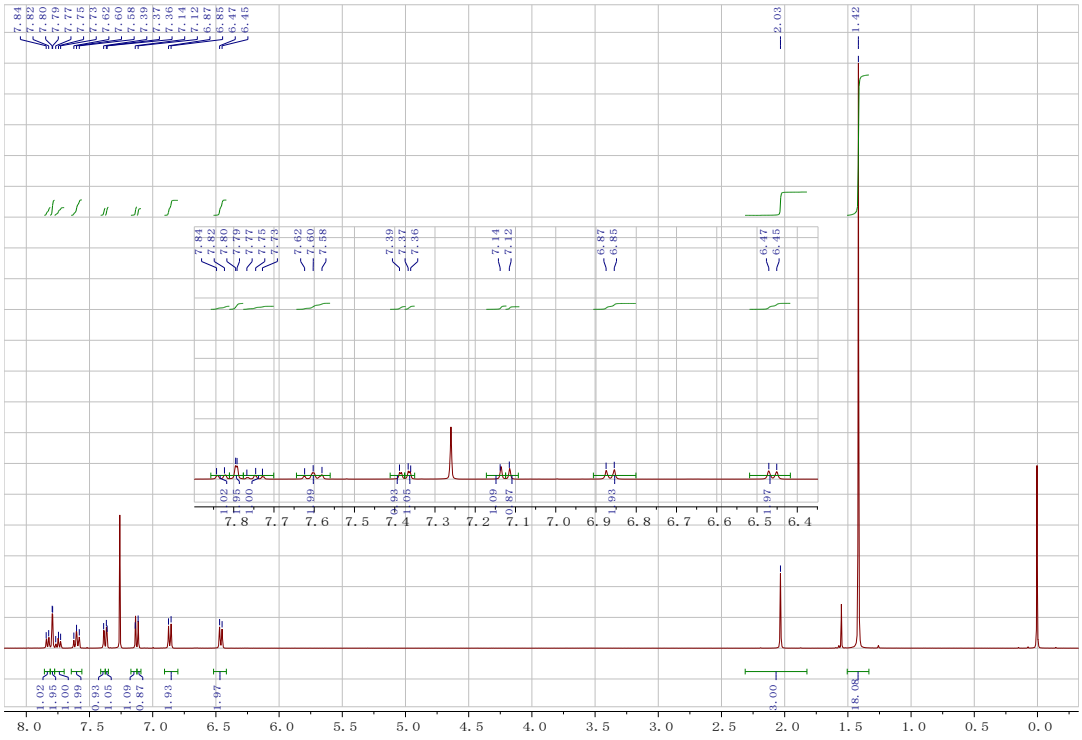

Fig. S11 ^{1}H NMR spectrum of *o*-tCz-BP.

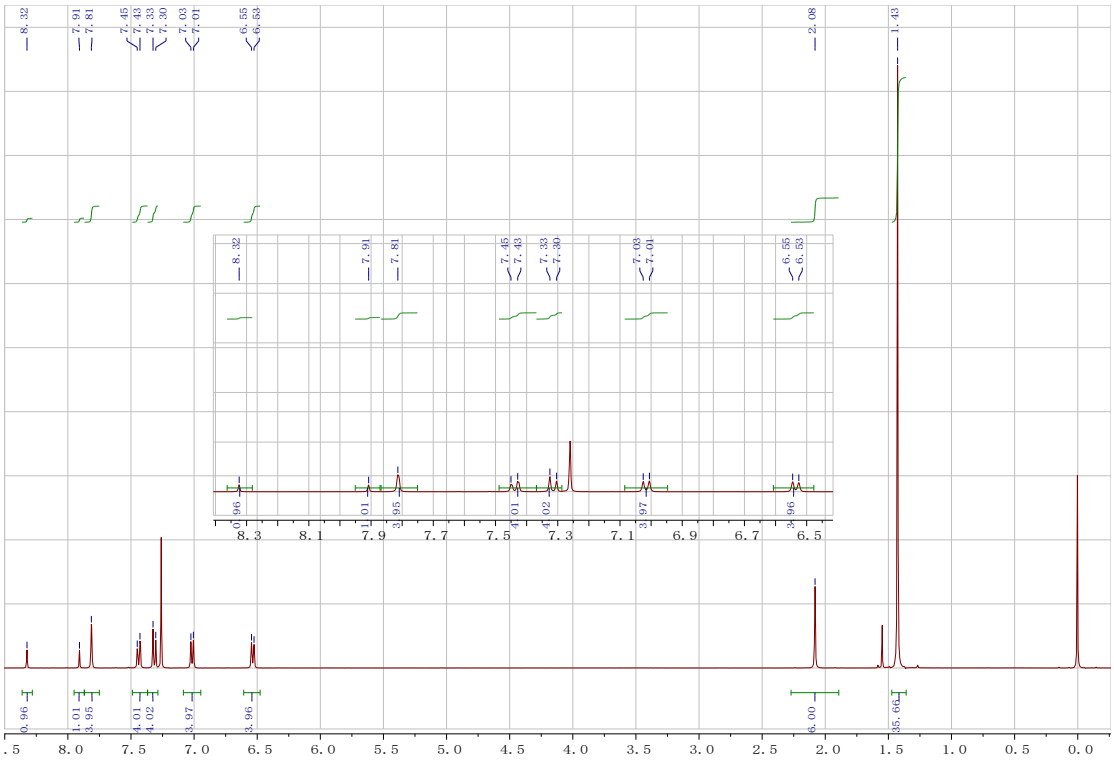

Fig. S12 ^{1}H NMR spectrum of D-tCz-D-BP.

4. References

1 T. Lu and F. Chen, *J Comput Chem*, 2012, **33**, 580-592.

2 T. Lu and Q. Chen, *J Comput Chem*, 2022, **43**, 539-555.

3 C. Lefebvre, G. Rubez, H. Khartabil, J. C. Boisson, J. Contreras-Garcia and E. Henon, *Phys. Chem. Chem. Phys.*, 2017, **19**, 17928-17936.

4 W. Li, B. Li, X. Cai, L. Gan, Z. Xu, W. Li, K. Liu, D. Chen and S. J. Su, *Angew. Chem., Int. Ed.*, 2019, **58**, 11301-11305.

5 R. Dong, J. Li, D. Liu, D. Li, Y. Mei, M. Ma and J. Jiang, *Adv. Opt. Mater.*, 2021, **9**,2100970.

6 T. Sudyoadsuk, S. Petdee, P. Chasing, P. Therdkatanyuphong, C. Kaiyasuan, W. Waengdongbung, S. Namuangruk and V. Promarak, *Dyes Pigm.*, 2021, **195**,109721.

7 Y. H. Lee, S. Park, J. Oh, S.-J. Woo, A. Kumar, J.-J. Kim, J. Jung, S. Yoo and M. H. Lee, *Adv. Opt. Mater.*, 2018, **6**,1800385.

8 H. L. Lee, W. J. Chung and J. Y. Lee, *Small*, 2020, **16**, 1907569.

9 X. Lv, Y. Wang, N. Li, X. Cao, G. Xie, H. Huang, C. Zhong, L. Wang and C. Yang, *Chem. Eng. J., 2020, **402**, 126173.*

10 T. Huang, Q. Wang, S. Xiao, D. Zhang, Y. Zhang, C. Yin, D. Yang, D. Ma, Z. Wang and L. Duan, *Angew. Chem., Int. Ed.*, 2021, **60**, 23771-23776.

11 M. Ouyang, L. Xing, Q. Chen, H. Huang, M. Zhu, K. Hu, Y. Liu, W.-C. Chen, Y. Huo and C. Yang, *J. Mater. Chem. C*, 2021, **9**, 1678-1684.

12 Y. Huang, D.-H. Zhang, X.-D. Tao, Z. Wei, S. Jiang, L. Meng, M.-X. Yang, X.-

L. Chen and C.-Z. Lu, *Dyes Pigm*., 2022, **204**, 110397.

13 H.-Z. Li, F.-M. Xie, K. Zhang, Y. Shen, W. Zhou, Y.-Q. Li, W.-J. Wang and J.-X. Tang, *Chem*. *Eng*. *J*., 2022, **436**,135234.

14 X. Zheng, R. Huang, C. Zhong, G. Xie, W. Ning, M. Huang, F. Ni, F. B. Dias and C. Yang, *Adv*. *Sci*., 2020, **7**, 1902087..

15 Z. Yang, Z. Mao, C. Xu, X. Chen, J. Zhao, Z. Yang, Y. Zhang, W. Wu, S. Jiao, Y. Liu, M. P. Aldred and Z. Chi, *Chem*. *Sci*., 2019, **10**, 8129-8134.

16 H. Chen, H. Liu, P. Shen, J. Zeng, R. Jiang, Y. Fu, Z. Zhao and B. Z. Tang, *Adv*. *Opt*. *Mater*., 2021, **9**,2002019.

17 J. Zeng, J. Guo, H. Liu, Z. Zhao and B. Z. Tang, *Adv. Funct. Mater.,* 2020, **30**,2000019.

18 Y.-K. Wang, Q. Sun, S.-F. Wu, Y. Yuan, Q. Li, Z.-Q. Jiang, M.-K. Fung and L.-S. Liao, *Adv. Funct. Mater.,* 2016, **26**, 7929-7936.

19 D. Liu, D. Li, H. Meng, Y. Wang and L. Wu, *J. Mater*. *Chem. C*, 2019, **7**, 12470-12481.